Spectral Patterns of Isomerizing Systems‡

Shuangbo Yang,§ Vivian Tyng, and Michael E. Kellman*

Department of Chemistry and Institute of Theoretical Science, University of Oregon, Eugene, Oregon 97403

Received: December 18, 2002; In Final Form: July 14, 2003

Spectral patterns are investigated in a model of an isomerizing coupled stretch-and-bend system that is intended to have some of the features of a realistic model of the acetylene−vinylidene isomerization. There are patterns of a dip or minimum in the spacing of neighboring energy levels, which is characteristic of the barrier, the multiple minima, and above-barrier motion. The patterns are obtained by classifying sequences in terms of approximate effective quantum numbers, which are determined using a diabatic correlation diagram technique. The patterns have anomalies that carry dynamical information that is associated with nonlinear resonance-type couplings, similar to anharmonic Fermi resonances, between the stretch and the bend. There is conventional Fermi resonance below the barrier, and a new type of "cross-barrier" resonance is observed.

1. Introduction

There is growing use of frequency-domain spectral analysis to unravel dynamical information about vibrating molecules.[1−15] This interest has progressed from motion near the bottom of a potential well to systems that approach barriers to molecular rearrangement. The observation in frequency-domain spectra of species with multiple potential minima, undergoing isomerization, is awaited with great interest. An example is the formation of the vinylidene isomer in the much-studied acetylene spectral system. Ideally, one would like to use the spectra to detect the presence of the barrier to isomerization, motion over the barrier, trapped quantum states of the above-barrier and isomerized species, and dynamics of the isomerization process. Despite impressive experimental and theoretical work,[16−25] it is fair to say that this area of study is mostly unexplored territory that holds many mysteries.

This paper investigates the existence and interpretation of spectral patterns that are associated with isomerization phenomena. It is known that there are spectral patterns[7,11,14] associated with *dynamical* barriers[26−29] in simple coupled systems, e.g., stretches with local and normal modes, and Fermi resonance. Furthermore, these patterns persist in molecular systems that have multiple resonances, many degrees of freedom, and classical chaos.[30−33]

It is natural to wonder if similar patterns exist in isomerizing systems with real potential barriers. In this paper, we investigate a simple two-mode stretch−bend model for an isomerizing system. This model is intended to have some features of a realistic model for the acetylene−vinylidene isomerization, including the critical features of a barrier between the acetylene and vinylidene wells, and motion above the barrier. The simplification to a two-mode model makes tractable a comprehensive investigation of key questions of principle. Are there spectral patterns that are characteristic of the barrier, the multiple minima, and above-barrier motion? Do they give information about the chaotic motion and energy-transfer dynamics, including movement between isomeric species?

This paper focuses on the question of spectral patterns of the acetylene, vinylidene, and above-barrier species. The full spectral interpretation of the isomerization kinetics is more subtle and is left for future investigation.

Jacobson and Child[34,35] investigated a model of spectroscopic signatures of bond-breaking internal rotation in a spherical pendulum model for a system with a barrier. There are several points of contact with the present work, which are described below.

The paper is organized as follows. We introduce the bend potential, stretch potential, and stretch−bend Hamiltonian in Section 2. We consider classical dynamics for the stretch−bend Hamiltonian system in Section 3. We develop quantum mechanical calculations for this Hamiltonian in Section 4. In Section 5, we discuss spectral patterns of the zero-order system, and in Section 6, patterns of the coupled system are explored. In Section 7, we discuss dynamical interpretation of the spectral patterns.

2. Bend−Stretch Isomerization Hamiltonian

We want the model stretch−bend Hamiltonian to include three main elements. First, we want a realistic HCC bend potential with a deep acetylene well and shallow vinylidene well, with motion in both wells and above the barrier. Second, we want a stretch mode that has some of the features of a C−H stretch, in particular, a frequency ratio between the stretch and the bend that is similar to that in acetylene. Finally, we want a semirealistic coupling between the stretch and the bend.

2.1. Bend Potential. For the bending motion, we seek a model of a local HCC bend that is similar to what can be expected in acetylene−vinylidene along the reaction coordinate. For this model, we use a realistic, full-degree-of-freedom acetylene potential energy surface (PES) and determine the potential along the reaction path.[36] We use the resulting one-dimensional potential, which is suitably parametrized, as our bend potential.

As a comprehensive ab initio PES of the acetylene−vinylidene system, with all vibrational degrees of freedom, we use the potential of Halonen, Child, and Carter.[37,38] Its stationary

‡ Part of the special issue "A. C. Albrecht Memorial Issue".

* Author to whom correspondence should be addressed. E-mail: kellman@oregon.uoregon.edu.

§ Permanent address: School of Physical Science and Technology, Nanjing Normal University, Nanjing 210097, PRC.

10.1021/jp027763o CCC: $25.00
Published on Web 09/13/2003

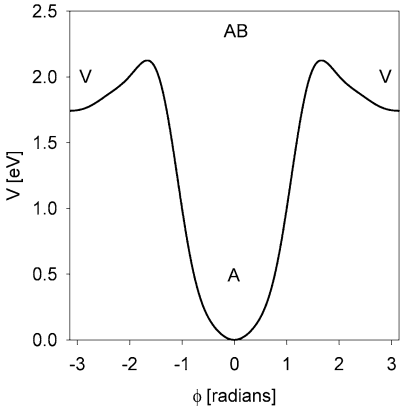

Figure 1. Bend potential obtained from fitting the reaction path abstracted from a full-dimensional ab initio surface for the acetylene system. Regions are denoted A (acetylene), V (vinylidene), and AB (above barrier).

points (acetylene, vinylidene, and the transition state) have been computed by Bentley et al.[39]

To obtain the reaction path, we start from the transition state with a tiny displacement toward either acetylene or vinylidene and then follow the path of steepest descent on the analytical PES. The result is a numerical representation of potential energy (given in terms of electron volts) versus a mass-weighted reaction coordinate (given in angstroms).[36]

For our purposes, it will be more suitable to switch to an angle parameter ϕ along the reaction path with a period of 2π. To define this parameter, we rescaled the aforementioned mass-weighted reaction coordinate linearly to a new variable ϕ ($\phi = [-\pi,\pi]$); for this variable, acetylene corresponds to $\phi = 0$ and vinylidene corresponds to $\phi = \pi, -\pi$. The potential was then fit using a least-squares routine (from MATHEMATICA) to a polynomial function of cos [ϕ] with the desired periodicity and symmetry. The final result is the following one-dimensional double-minimum bend potential:

$$V(\cos\phi) = 2.106983 - 0.441741\cos\phi - 2.76936\cos^2\phi - 2.28737\cos^3\phi + 2.30354\cos^4\phi + 3.11721\cos^5\phi - 0.769832\cos^6\phi - 1.25943\cos^7\phi \quad (1)$$

where the result is given in electron volts. The potential, $V(\cos\phi)$, is shown in Figure 1. Periodic in regard to ϕ, it has a well at $\phi = 0$ for acetylene and a shallow well at $\phi = \pi, -\pi$ for vinylidene.

2.2. Stretch Potential. We assume the potential model for the C−H stretch to be a Morse oscillator:

$$V_s = D(1 - e^{-\beta r})^2 \quad (2)$$

where D is the dissociation energy for the C−H bond, β the Morse parameter, and r the displacement from equilibrium of the C−H bond.

2.3. Stretch−Bend Interaction. For the coupling between the stretch and the bend, we take a potential coupling of the form

$$V_{sb} = \kappa r \sin^2\phi \quad (3)$$

which, to first order, would give a 2:1 Fermi resonance interaction. In the stretch−bend system, the kinetic-energy coupling to first order is known to give a coupling of this form.[40] Our model Hamiltonian for bend, stretch, and coupling then is

$$H = \frac{p_r^2}{2m} + D(1 - e^{-\beta r})^2 + \frac{p_\phi^2}{2m_H r_0^2} + V(\cos\phi) + \kappa r \sin^2\phi \quad (4)$$

where r_0 is the equilibrium C−H bond length, r the displacement from equilibrium for the C−H bond; m the reduced mass of the H and C atoms; m_H the mass of the H atom; and κ an adjustable coupling constant.

This model is a deliberate oversimplification in certain respects, besides being restricted to two dimensions. The double-well potential (eq 1) for the bend has only a single form for each species, unlike the real acetylene−vinylidene system. Furthermore, in acetylene−vinylidene, the properties of the C−H stretch mode, e.g., its zero-order frequencies, are different for the two species. To reflect this in a potential model, the stretch potential would need to be a function of both the stretch and bend coordinates, unlike the potential that is dependent only on the stretch coordinate (eq 2), with all the dependence on the bend coordinate folded into the stretch−bend potential (eq 3), which is, itself, a simple functional form.

3. Classical Dynamics

In this section, we compute classical dynamics of the Hamiltonian system (eq 4). For convenience in numerical calculation, we rescale the variables in eq 4 to dimensionless form. To do this, we introduce the length coordinate w for the bend, which relates to the bending angle ϕ by the equation $w = r_0\phi$. The momentum p_w conjugate to w relates to the angular momentum p_ϕ by $p_\phi = r_0 p_w$. The Hamiltonian shown in eq 4 then becomes

$$H = \frac{p_r^2}{2m} + D(1 - e^{-\beta r})^2 + \frac{p_w^2}{2m_H} + V\cos\left(\frac{w}{r_0}\right) + \kappa r \sin^2\left(\frac{w}{r_0}\right) \quad (5)$$

Equation 5 can then be scaled to the form

$$\epsilon = \frac{1}{2}\tilde{p}_r^2 + (1 - e^{-x})^2 + \frac{1}{2}\left(\frac{m}{m_H}\right)\tilde{p}_w^2 + \frac{1}{D}V\cos\left(\frac{y}{x_0}\right) + \frac{A_{sb}}{D}x\sin^2\left(\frac{y}{x_0}\right) \quad (6)$$

by the transformations

$$x = \beta r$$
$$\tilde{p}_r = \frac{p_r}{\sqrt{mD}}$$
$$y = \beta w$$
$$\tilde{p}_w = \frac{p_w}{\sqrt{mD}}$$
$$\tau = D\gamma t \quad (7)$$

where

$$x_0 = \beta r_0$$
$$\gamma = \sqrt{\frac{\beta^2}{mD}}$$
$$A_{sb} = \frac{\kappa}{\beta} \quad (8)$$

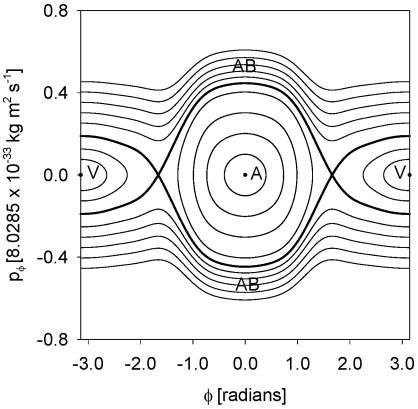

Figure 2. Phase space trajectories for motion in the bend potential of eq 1. Classical motion is organized around the acetylene potential minimum (A), the vinylidene potential minimum (V), and the above-barrier region (AB) outside the separatrix (bold trajectory), corresponding to the top of the isomerization barrier.

and t is the time for Hamiltonian eq 5. The scaled variables x, x_0, $\tilde{p}_r$, y, $\tilde{p}_w$, and τ are dimensionless quantities.

Classical trajectories are computed by numerically solving the equations of motion for Hamiltonian eq 6 with the following parameters being explicit or implicit:

$$D = 47474.26\ \text{cm}^{-1}$$

$$\omega_s = \sqrt{\frac{2D\beta^2}{m}} = 3459.59\ \text{cm}^{-1}$$

$$\frac{\hbar^2}{2m_H r_0^2} = 1.838 \times 10^{-3}\ \text{eV} = 14.82481174\ \text{cm}^{-1}$$

$$A_{sb} = 10904.4\ \text{cm}^{-1} \qquad (9)$$

The reasons for this particular choice of parameters are detailed in the Appendix.

Figure 2 shows phase−space trajectories for the pure bend at different energies. There are curves that surround fixed point **A** at the bottom of the deep acetylene well, curves that surround fixed point **V** at the bottom of the shallow vinylidene well, and curves that extend over the full range $\phi = [-\pi, \pi]$ in the above-barrier region **AB**.

Figure 3a shows a surface of a section for the coupled system obtained at an energy of 18 800 cm^{-1}, which is the approximate energy of the barrier when the system has $n_s = 0$ stretch quanta, including zero-point energy. A region of mild chaos surrounds the separatrix. There is a pronounced four-island chain in the acetylene well. It corresponds to the ∼4:1 frequency ratio of the zero-order stretch and bend of the model system, as discussed below in Section 4.1, and it thereby corresponds to the 4:1 Fermi resonance that is discussed in Section 7.1. The surfaces of sections at 29 000 cm^{-1} in Figure 3b and 35 300 cm^{-1} in Figure 3c correspond approximately to the barrier energy for states with $n_s = 3$ and 5 stretch quanta and show a progressively higher degree of chaos that surrounds the separatrix. The 2:1 Fermi resonance that corresponds to the form of the coupling presented in eq 3 eventually turns on, as seen in Figure 3c.

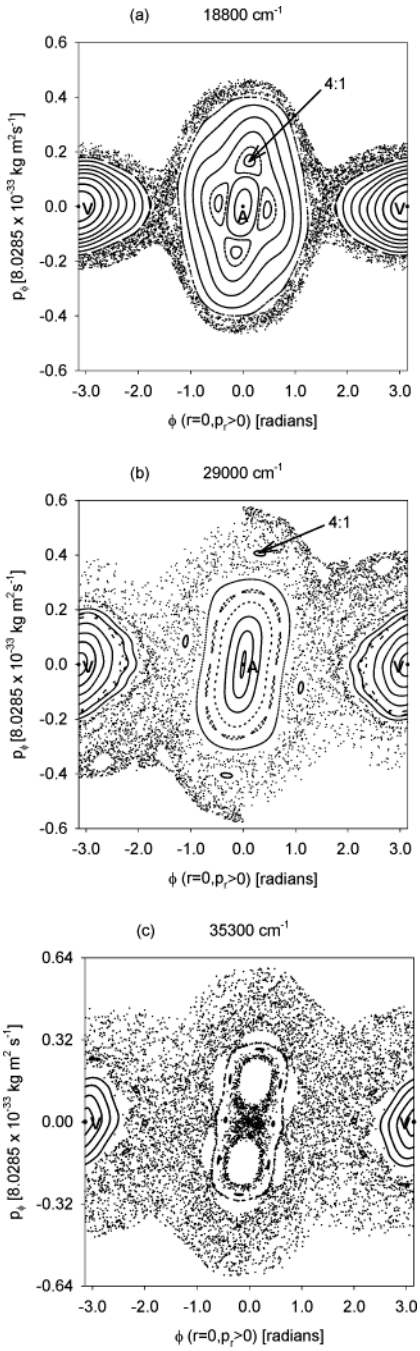

Figure 3. (a) Surface of a section at $r = 0$, $p_r > 0$ for the coupled stretch−bend Hamiltonian eq 4 at a total energy (including zero-point energy) of (a) $E = 18\,800\ cm^{-1}$, (b) $E = 29\,000\ cm^{-1}$, and (c) $E = 35\,300\ cm^{-1}$. These energies correspond to the approximate energies at the barrier for the sequences $n_s = 0$, 3, and 5, respectively. Note that the sequences depicted in Figures 6−9 do not include the zero-point energy.

4. Quantum Calculations

In this section, we calculate the quantum states of the Hamiltonian eq 4. The quantum calculations have two steps. The first is to calculate eigenvalues and eigenfunctions for the double-well bend potential (eq 1) in a large free-rotor basis. The second is to calculate the states of the coupled stretch−bend system. For this step, the states of the preceding bend calculation give a prediagonalized zero-order bend basis. Together with a basis of Morse functions for the zero-order stretch, these form a product zero-order stretch−bend basis, which is used finally to calculate the states of the coupled system (eq 4).

4.1. States of the Double-Well Bend Potential. The states of the bend potential are obtained by solving the Schrödinger equation:

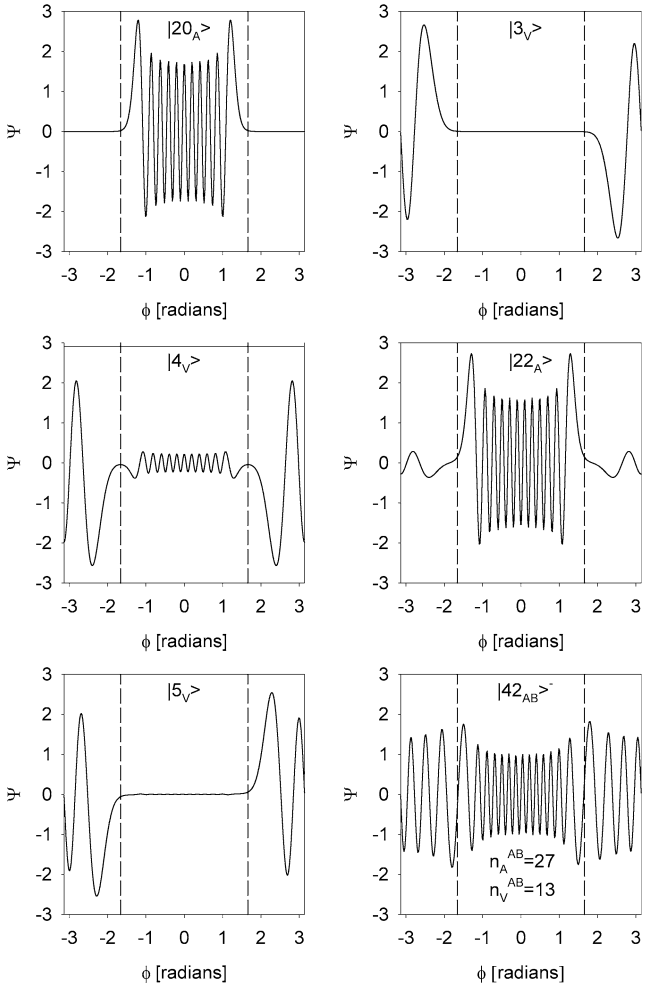

Figure 4. Selected eigenfunctions of the double-well bend potential of Figure 1. Each state is labeled with the appropriate quantum number n_A, n_V, or n_{AB}, depending on its acetylene, vinylidene, or above-barrier character, respectively. The above-barrier state $|42_{AB}\rangle^-$ is also labeled with the pseudo-quantum numbers n_A^{AB}, n_V^{AB}. The bend quantum numbers are described in Section 4.1. The vertical dashed lines indicate the top of the barrier to isomerization, and the above-barrier function shown for $|42_{AB}\rangle^-$ is the real portion of the eigenfunction.

$$\hat{H}_b\psi_b = E_b\psi_b \tag{10}$$

where, using the bend portion of the classical Hamiltonian eq 4, we get

$$\hat{H}_b = -\frac{\hbar^2}{2m_H r_0^2}\frac{d^2}{d\phi^2} + V(\cos\phi) \tag{11}$$

Because $V(\cos\phi)$ is a periodic function of ϕ, we choose, as a basis set, the function

$$\frac{1}{\sqrt{2\pi}}e^{il\phi} \tag{12}$$

for $l = 0, \pm1, \pm2, \pm3, ...$ Using the parameters of eq 9, we find 24 acetylene states below the barrier of the potential $V(\cos\phi)$ and 8 vinylidene states within the shallow second well. We diagonalize $\hat{H}_b$ in the first 201 basis states, i.e., up to $|l| = 100$, and retain, for later use, the converged eigenenergies $E_b(n_b)$ and eigenfunctions:

$$\psi_{n_b}(\phi) = \frac{1}{\sqrt{2\pi}}\sum_{l=-100}^{100} c_{n_b}^{l} e^{il\phi} \tag{13}$$

for $n_b = 1, 2, 3, ..., 80$. The n_b terms label the eigenenergies in ascending order; therefore, n_b is not a physically meaningful quantum number, but rather is simply an index.

Physical quantum numbers can be discerned by examining the bend eigenfunctions. A sampling of wave functions is shown in Figure 4, with relevant quantum number assignments. Below the vinylidene well, the states are strongly localized in the acetylene well and characterized by the number of quanta n_A in the acetylene bend. As the energy reaches the vinylidene well, states that are localized in the vinylidene well start to appear, which are characterized by the number of vinylidene bend quanta, n_V. Significant mixing of states with A and V character begins, which can be thought of as being due to tunneling between the two isomeric forms. This can be observed in the middle panels of Figure 4, which show unusually large tunneling mixing. Nonetheless, all the states are predominantly of either A or V character almost up to the top of the barrier and can be characterized by the bend quantum number n_A or n_V.

The wave functions of the above-barrier states are complex, which befits a system with rotation about the full angular range $[-\pi, \pi]$. In Figure 4, we plot the real portion of the wave functions for the above-barrier states. (The wave functions are predominantly real, up to a point far above the barrier; the same will be true of the wave functions of the coupled system at the energies that we will consider.)

Above the barrier, states are characterized by a new bend quantum number, n_{AB}, which is determined by the number of nodes in the real portion of the wave function. These states come in pairs, corresponding to the twofold direction of hindered rotation above the barrier. (There is one state just below the barrier that is difficult to characterize; however, this state is best thought of as a member of the first above-barrier pair.) These pairs coalesce into near-degenerate doublets as the energy increases above the barrier.

There is another, approximate way to characterize the real portion of the above-barrier states that is very useful. For quite a distance above the barrier, the states have strongly oscillating amplitude above both the acetylene and vinylidene wells. It is possible to ascribe to the states approximate numbers of acetylene and vinylidene quanta. Consider state $|42_{AB}\rangle^-$ in Figure 4. The dashed lines indicate the location of the barrier. Counting the number of nodes within the acetylene "box", one can ascribe an approximate or pseudo-quantum number of "acetylene" bend quanta: $n_A^{AB} = 27$. Similarly, by counting the number of nodes within the vinylidene "box", one can ascribe an approximate number of "vinylidene" bend quanta: $n_V^{AB} = 13$. These above-barrier quantum numbers will be useful later in interpreting anomalies in spectral patterns of the coupled system.

We assign the states of the uncoupled stretch−bend system with these quantum numbers. For example, the state with $n_s = 2$, $n_A = 15$ is denoted as $(n_s, n_A)_0 = (2_s, 15_A)_0$. The subscript "0" denotes the fact that these states of the uncoupled system will be the zero-order basis states of the coupled system. Vinylidene states are denoted as $(n_s, n_V)_0$. Above-barrier states are denoted in two ways: as $(n_s, n_{AB})_0^{\pm}$; or in terms of the very approximate quantum numbers n_A^{AB} and n_V^{AB}, as $(n_s, n_A^{AB}, n_V^{AB})_0^{\pm}$.

Using the model bend potential expressed in eq 1, the ratio of the stretch and bend frequencies is ~4:1, rather than the ~5:1

ratio that is observed experimentally in acetylene. The reason for this difference is that the model bend potential comes from fitting a reaction path on an ab initio potential surface.

4.2. Coupled Stretch−Bend States. We now compute states of the stretch−bend system by diagonalizing the Schrödinger equation for the Hamiltonian eq 4 in a product basis of zero-order stretch−bend states $(n_s, n_b)_0$ that is given by

$$(n_s, n_b)_0 = \psi_{n_s}(x)\psi_{n_b}(\phi) \tag{14}$$

with $x = \beta r$ for $n_s = 1, 2, 3, ..., N_s$ and $n_b = 1, 2, 3, ..., N_b$, with n_b being the label that has been described previously, following eq 13. Here, the stretch basis states $\psi_{n_s}(x)$ are eigenfunctions for the Morse oscillator and the bend basis states $\psi_{n_b}(\phi)$ are the eigenfunctions that have been computed previously for the double-well bend potential; it is understood that the bend states ψ_{n_b} can be classified by the physical quantum numbers n_A, n_V, n_{AB}, etc. that have been described previously. Using the parameter values of eq 9, the number of bound states in the Morse potential is $N_s = 27$; the number of bend eigenstates taken from the set computed previously for the bend is $N_b = 80$, with 32 below barrier (24 acetylene and 8 vinylidene) and the remainder above barrier.

In constructing and diagonalizing the Hamiltonian eq 4, known properties of the eigenvalues and eigenfunctions of the one-dimensional Morse oscillator are used.[41−44] Of course, the $\psi_{n_b}(\phi)$ bend basis functions are available only numerically, from the calculation described in Section 4.1. The diagonal matrix elements $\langle\psi_{n_s}|x|\psi_{n_s}\rangle$ for $n_s = 1, 2, 3, ..., N_s$ for the Morse oscillator are obtained using the numerical integration method for reducing the round-off error described in ref 42; analytical results are available but are difficult to implement numerically, as discussed in ref 42. The off-diagonal matrix elements are computed analytically, as given in ref 43.

5. Spectral Patterns: Uncoupled System

We first consider spectral patterns of the uncoupled stretch−bend system. We will use these as the template for patterns of the coupled system.

Energy levels of the uncoupled system can be classified into bend sequences $(n_s, n_b) = (n_s, 0), (n_s, 1), ...$, according to the number of stretch quanta in the sequence. Analogous to refs 7 and 11, for each sequence, we examine the pattern of energy differences between adjacent energy levels, i.e., $E(n_s, n_b + 1) - E(n_s, n_b)$ versus $E(n_s, n_b)$ for $n_b = 1, 2, 3, ..., 50$ for each sequence. The pattern for the sequence $(n_s = 0, n_b)$ is shown in Figure 5a. Of course, the patterns for sequences with $n_s = 1, ...$ are identical for the *uncoupled* system, except for being displaced to higher energies.

A more revealing pattern is obtained when the vinylidene states are removed. This leaves the spacings for acetylene levels with quantum number n_A, and above-barrier levels with quantum number n_{AB}. These are plotted in Figure 5b. It is clear now that there is a minimum or dip that corresponds classically to the zero frequency of the bend at the barrier. It is known (see Figure 5 of ref 7) that, at a classical separatrix, there is a pattern of a dip in the spacings between levels of a vibrational *polyad*, similar to the pattern that is shown here in Figure 5b. Furthermore, it is known that there is a formal connection between the phase space separatrix structure and "dynamical barriers".[26−29] In the present case, the barrier that gives the separatrix is the actual barrier to isomerization in the double-well potential. In a system with a potential barrier, the minimum was studied by Dixon.[45] The "Dixon dip" is noted by Jacobson and Child for their zero-order spherical pendulum model in Figure 5 of ref 34.

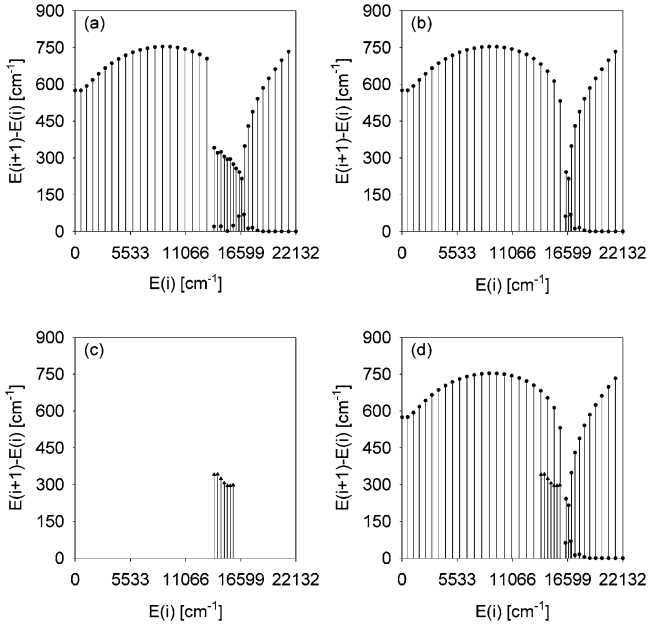

Figure 5. (a) Pattern of energy-level spacings for the uncoupled bend−stretch system; (b) energy-level pattern excluding states localized in the vinylidene well; (c) spacing pattern of the vinylidene states alone; (d) patterns of panels b and c superimposed.

Figure 5c shows the pattern of energy-level spacings for the vinylidene states alone. Figure 5d shows the pattern when the spacings of the vinylidene states are superimposed on the previous "dip" pattern of acetylene and above-barrier states. The reason for doing this is that, in some cases (see Figure 6 of ref 7 and Figure 9a of ref 11), instead of a dip in the level spacings, there is an interleaving "fan" or "zigzag". In the Fermi resonance system, the fan is similar to (but simpler than) the pattern shown here in Figure 5a. In the Fermi system, the fan can be "straightened" by a proper assignment procedure (see Figure 8 of ref 7). This is analogous to plotting the spacings of the (n_A, n_{AB}) levels in one group and those of the n_V group in another, as we did in Figure 5d of the current work. In the Fermi resonance system, a strikingly simpler pattern results from the straightening procedure (see Figure 8 of ref 7, Figure 9b of ref 11). In comparison, Figure 5d is not simplified as much. The reason involves the special form of the Fermi resonance interaction: in particular, in the Fermi system, the coupling corresponds to a single trigonometric term, in contrast to the double-well potential used here, which has several terms in the trigonometric function expansion of eq 1.

6. Spectral Patterns: Coupled System

Panels b and c of Figure 5 show the uncoupled stretch−bend system, which form the basic template of spectral patterns that we will use to organize the spectrum of the coupled system. We will attempt to classify sequences of levels that are characterized by approximate effective quantum numbers analogous to n_s, n_A, n_V, and n_{AB} and compare the energy patterns of the resulting sequences to those of the uncoupled system in Figure 5.

6.1. Diabatic Correlation Diagram Assignment of Sequences. The first thing we need to do is assign approximate quantum numbers to the energy levels, so that we can classify the spectrum into sequences. For this step,we use the diabatic correlation diagram assignment method of Rose and Kellman.[30]

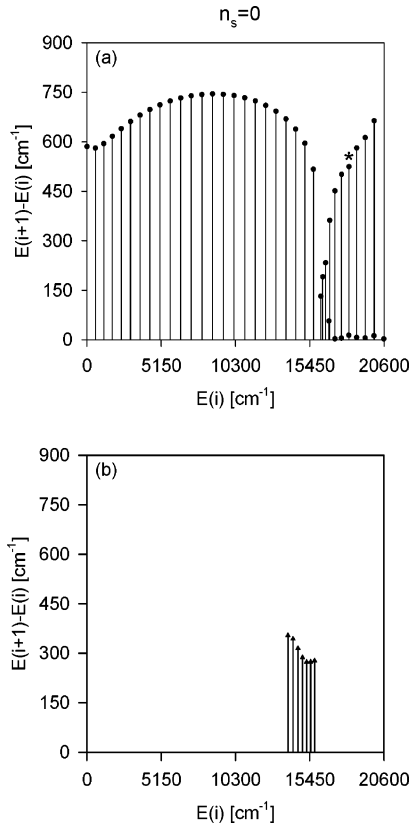

Figure 6. Energy-level spacing patterns for the coupled system with $n_s = 0$ stretch quanta. Panels a and b parallel panels b and c of the uncoupled system in Figure 5. The spacing marked with an asterisk (*) is involved in a cross-barrier, resonance-type coupling, as described in Section 7.2.

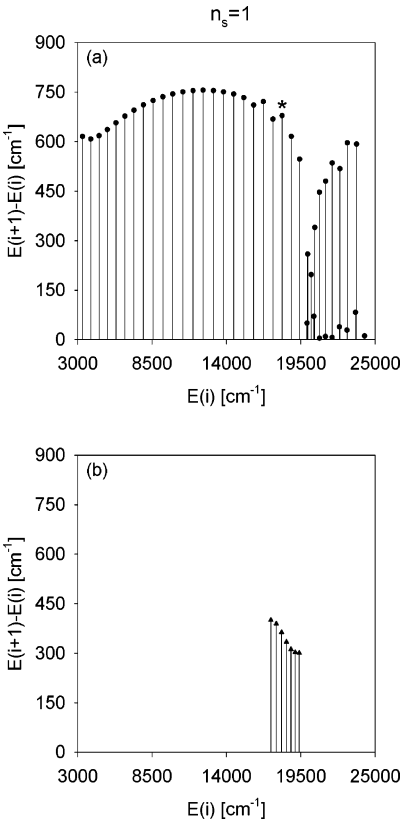

Figure 7. Energy-level spacing patterns for the coupled system with $n_s = 1$ stretch quanta. Panels a and b parallel panels b and c of the uncoupled system in Figure 5. The spacing marked with an asterisk (*) is involved in a cross-barrier, resonance-type coupling, as described in Section 7.2.

We start with the precisely defined quantum numbers of the uncoupled system. We then gradually turn on the coupling, carrying the zero-order quantum numbers along the diabatic curves of the correlation diagram. The intuitive expectation is that the character of the states does not change too rapidly as the coupling is turned up, so that the zero-order quantum numbers retain some physical meaning as the coupling is increased. This expectation rests partly on prior favorable experience in both direct applications of the method[30−33] and in related work where correlation diagrams are used.[9,12,13] The test of utility here is whether the procedure uncovers meaningful patterns in the fully coupled system.

6.2. Energy-Level Patterns. After approximate effective quantum numbers have been assigned to the states of the coupled system, we arrange the levels into sequences (n_s, n_b), analogous to those of the uncoupled system with quantum numbers $(n_s, n_b)_0$ in Section 5, and also making use, where appropriate, of the various quantum numbers n_s, n_A, n_V, n_{AB}, n_A^{AB}, and n_V^{AB}, analogous to the zero-order counterparts that were described previously. We examine the patterns of energy-level spacings, analogous to Figure 5; the results are shown in Figures 6−9 for sequences with various values of the effective stretch quantum number ($n_s = 0-3$). We were readily able to assign these sequences using the correlation diagram technique. Even up to $n_s = 5$, we were able to assign all the acetylene and vinylidene levels below the barrier, except possibly one. However, the assignments became unmanageable above the barrier, showing the limits of the diabatic correlation diagram technique when the degree of chaos is too high. (See discussion in Section 3 and the classical surfaces of the section shown in Figure 3.)

Figure 6 shows $n_s = 0$, with panels a and b analogous to panels b and c in Figure 5. Evidently, the patterns of the uncoupled and coupled systems are essentially similar, which confirms the basic hypothesis with which we started this investigation. However, there is apparently some "bumpiness" in the pattern above the barrier. This phenomenon is visible repeatedly in Figures 7−9. The irregularities persist and generally grow in magnitude with increasing n_s; the figures show bumps both above and below the barrier. It will become clear that these irregularities signal important dynamical information.

7. Decoding the Spectral Patterns

We will start with familiar ideas from molecular vibrational spectroscopy and, motivated by concepts from kinetic theory, we will attempt to extend these to encompass the fact that an isomerizing system is involved in our study. The main idea from molecular spectroscopy is the notion of Fermi or anharmonic resonance. We will classify the anomalies in Figures 6−9 and interpret several exemplary cases, highlighting the association with resonances. The basic concept from the kinetic theory of unimolecular reactions[46] is to treat the isomerization process as the formation of an activated form $A^\dagger$ of the energized acetylene species A^*, followed by the transition to vinylidene:

$$A^* \rightleftharpoons A^\dagger \rightleftharpoons V \tag{15}$$

where the above-barrier form AB is considered to be the activated species $A^\dagger$, and A^* is an energized acetylene molecule with energy sufficient to form $A^\dagger$ but not properly localized in the reaction coordinate.

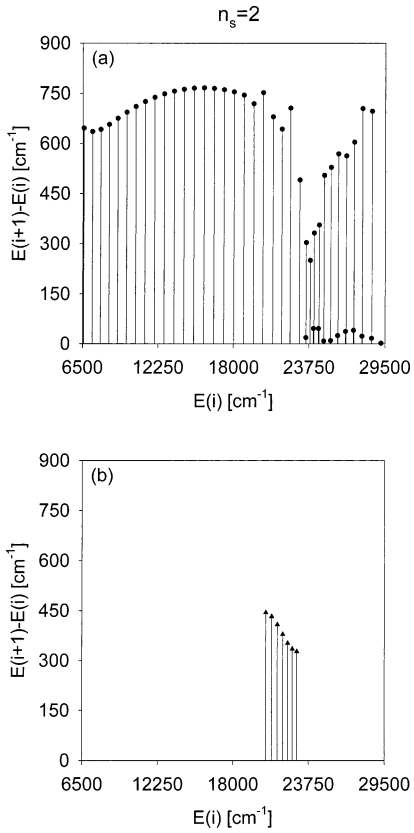

Figure 8. Energy-level spacing patterns for the coupled system with $n_s = 2$ stretch quanta. Panels a and b parallel panels b and c of the uncoupled system in Figure 5.

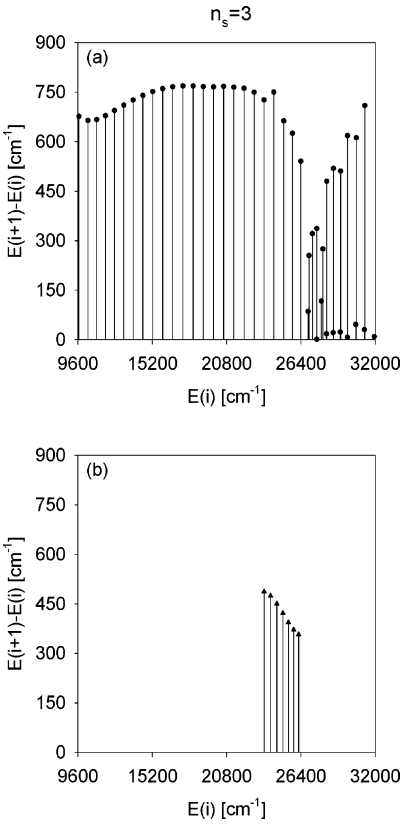

Figure 9. Energy-level spacing patterns for the coupled system with $n_s = 3$ stretch quanta. Panels a and b parallel panels b and c of the uncoupled system in Figure 5.

7.1. Fermi Resonance of Acetylene. First, we consider a spectral anomaly that has been interpreted in terms of ordinary Fermi resonance coupling among zero-order below-barrier acetylene states. In comparing Figure 5 for the zero-order system with Figure 9 for the coupled system with $n_s = 3$, a "wave" of slightly displaced states (n_s, n_A) is visible below the barrier.

In examining the eigenvectors of these states, we find that there is strong mixing of zero-order states that are connected by couplings of the form 4:1 and 2:1, i.e., exchanging 4 or 2 quanta of acetylene bend, respectively, for 1 quantum of stretch. This coupling is consistent with what we know of the classical dynamics of the system. To the lowest order, the coupling eq 3 has the form of a 2:1 coupling. Furthermore, the two lowest-energy surfaces of the section in Figure 3 have prominent 4:1 resonance zones, which is expected because the system tunes into a frequency ratio of ~4:1 between the stretch and the bend in the upper half of the bend potential, as noted in Section 4.1. The 2:1 and 4:1 resonances, and their interplay, were also investigated extensively by Child and Jacobson in their study of the spherical pendulum model of isomerization.[34,35]

However, the strong 4:1 mixing of the zero-order states is not yet analogous to what is generally meant by Fermi resonance. In molecular spectroscopy, the "zero-order" states of the diagonal portion of an effective fitting Hamiltonian are strongly mixed states in terms of any simple basis, such as our zero-order basis. Instead, the spectroscopic zero-order states are akin to our diabatic states outside regions of a strong avoided crossing. The effective quantum numbers (n_s, n_A) from the diabatic assignments are then similar to the zero-order quantum numbers of a spectroscopic Hamiltonian.

To establish that the displaced states are associated with 4:1 Fermi resonance in the spectroscopic sense, we place sets of states from sequences with different n_s numbers into 4:1 Fermi polyads of levels with a common polyad number of $P = 4n_s + n_A$. Figure 10 shows the energy-level spacings of a 4:1 polyad of states with effective quantum numbers of (1_s, 22_A),(2_s, 18_A), ..., (6_s, 2_A), all of which have a polyad number $P = 26$. Figure 10 displays a dip in the energy-level spacings, which is characteristic[7] of a separatrix. Now, the separatrix is associated not with the potential barrier that we have been considering in this paper, but rather with the dynamical barrier of a 4:1 nonlinear resonance.

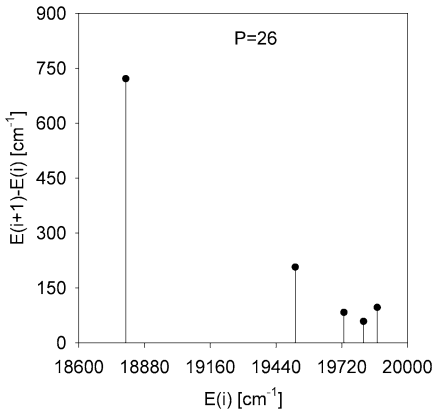

Figure 10. Pattern of five energy-level spacings of the polyad $P = 4n_s + n_A = 26$ of six states of the strong 4:1 resonance. The dip in the spacings corresponds to the separatrix of the 4:1 resonance.

It is also instructive to examine wave functions. Figure 11a shows the wave function of the state with nominal quantum numbers (n_s, n_A) = (4_s, 10_A) from the diabatic assignment. The nodal patterns are characteristic not of a state with quantum numbers (4_s, 10_A)$_0$, but rather of the stable periodic orbit of the classical 4:1 Fermi resonance, superimposed on the figure.

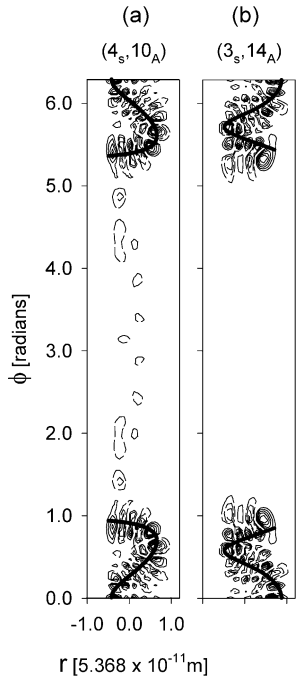

Figure 11. Real portion of the eigenfunctions of two Fermi resonant states: (a) state with nominal quantum numbers $(n_s, n_A) = (4_s, 10_A)$ tracks the stable periodic orbit of the 4:1 resonance, superimposed, and (b) state with nominal quantum numbers $(n_s, n_A) = (3_s, 14_A)$ tracks the unstable periodic orbit of the 4:1 resonance.

Figure 11b shows the wave function of state $(3_s, 14_A)$. The nodal patterns track the unstable orbit of the 4:1 resonance.

Figures 6−9 show that, even with Fermi coupling, it is meaningful to classify states into sequences that are assigned with nominal effective stretch and bend quantum numbers (n_s, n_A). We saw that these states could be further classified into Fermi polyads, as in Figure 10, with the help of the assignments. The presence of Fermi resonance is not surprising. What is significant is that the diabatic assignment still gives a sensible sequence classification and, in fact, helps to uncover resonance through the detection of anomalies in the spectral pattern. This demonstrated usefulness of the diabatic assignments gives us confidence to apply it to novel situations that involve coupling to above-barrier and isomeric species.

B. Cross-Barrier Coupling, $A^* \leftrightarrow A^\dagger$. Next, we consider a spectral anomaly that has a much more interesting explanation: as coupling of the excited acetylene species A^* to the activated complex $A^\dagger$. This can be interpreted as a type of generalization of Fermi resonance. Consider the energy spacing labeled by an asterisk (*) in Figure 7. This is the energy difference between the states $(n_s, n_A) = (1_s, 21_A)$ and $(1_s, 22_A)$, and this value clearly is "bumped" up from the general pattern. This observation means that the $(1_s, 21_A)$ level is anomalously low, the $(1_s, 22_A)$ level is anomalously high, or both. As we noted previously, the $(1_s, 22_A)$ level, in fact, is disturbed by 4:1 Fermi resonance with other below-barrier states. However, in addition, examination of the eigenvector $(1_s, 21_A)$ shows a strong admixture of the zero-order above-barrier basis state $(0, 42_{AB})_0^-$. This zero-order state, by the method of counting approximate above-barrier acetylene quanta of Section 4.1, is also assignable with the very approximate quantum numbers $(n_s, n_A^{AB})_0 = (0_s, 27_A^{AB})_0$. Furthermore, if we look at the spacing "*" between the states $(n_s, n_{AB})^\pm = (0, 42_{AB})^-$ and $(0, 43_{AB})^+$ in Figure 6, we find that it also is anomalously low. All this information suggests a Fermi resonance-type coupling between the acetylene state $(1_s, 21_A)$ and the above-barrier state $(0, 42_{AB})^- \approx (0_s, 27_A^{AB})_0$, exchanging 6 pseudo quanta of acetylene bend for 1 quantum of stretch, which resembles a resonance of order 6:1. The other anomalous "bumps" that are apparent on both sides of the barrier in Figures 6−9 can be interpreted in this way, with a resonance-type picture of the coupling between the species A^* and $A^\dagger$.

7.3. Isomerization and the Coupling to Vinylidene. A most interesting question is whether the spectral patterns in Figures 6−9 and the quantum mechanical calculations from which they resulted provide information about the isomerization process, including the right-hand portion $A^\dagger \rightleftharpoons V$ of the kinetic scheme of eq 15. Unfortunately, this is not as easily determined as the information that we have obtained of the Fermi resonance between acetylene states and the cross-barrier resonance-type interaction between acetylene and above-barrier states. The reason is obvious in Figures 6−9. The vinylidene states in panels b of the figures simply do not show the types of anomalies that allowed us to reach our earlier conclusions. This is a reflection of the weakness of the coupling of the vinylidene V species to the A^* and $A^\dagger$ forms of the system. Relating the present work on the $A^* \rightleftharpoons A^\dagger$ portion of the kinetic scheme of eq 15 to the process $A^\dagger \rightleftharpoons V$ will require more-subtle analysis of the quantum states and classical dynamics of the coupled system and is reserved for future investigation.

8. Summary and Conclusions

This paper has investigated the energy-level patterns in a model of an isomerizing coupled stretch-and-bend system that is intended to have some of the key features of a realistic model of the acetylene−vinylidene isomerization. We have seen that there are spectral patterns characteristic of the barrier, the multiple minima, and above-barrier motion. The patterns are obtained by classifying sequences in terms of approximate effective quantum numbers, which are obtained by a diabatic correlation diagram technique. The patterns are similar to those obtained earlier for nonisomerizing systems with Fermi resonance, which have phase space structure that is characterized by a classical separatrix, or dynamical barrier. As the dynamical barrier is approached from above or below, there is a characteristic pattern of a minimum, or dip, in the spacing between neighboring energy levels. In this study, we have found these types of patterns in the stretch−bend sequences of the model isomerizing system.

The patterns have anomalies or "bumps" in the energy-level spacing that carry significant dynamical information about the isomerizing system. Some of the anomalies are associated with standard Fermi resonance couplings between below-barrier states. Other anomalies are associated with a new type of cross-barrier resonance-type coupling, similar to Fermi resonance, that bridges below-barrier and above-barrier states, and takes the system from an energetically excited state to an activated form.

These results suggest several directions for future work, two of which we have mentioned. Most obviously, how to use the interpretation of the energy-level patterns to obtain information about the classical and quantum kinetics of the isomerization reaction remains to be seen.

Second, it would be extremely interesting if one could build a spectroscopic Hamiltonian, including resonances couplings for an isomerizing system, similar to the Hamiltonians commonly used to fit lower-energy spectra. This is difficult because of the need to incorporate the structures of both potential wells, the above-barrier form of the molecule, and resonance couplings, including the cross-barrier couplings that have been considered

here. Some real progress has been made[34,35] for two-mode models which, however, are much less similar to the acetylene−vinylidene system than the model studied here. The usefulness of the quantum numbers used in the present work in interpreting the dynamical meaning of the spectral patterns suggests that quantum numbers such as these will be an essential component of building a spectroscopic Hamiltonian for isomerizing systems.

Acknowledgment. This work was supported by the U.S. Department of Energy Basic Energy Sciences Program, under Contract No. DE-FG03-98ER14848. S.Y. was also supported by the educational committee of JiangSu province of China, under Project No. 2000WLX0002SJ1.

Appendix: Parameters of the Hamiltonian

In this Appendix, we indicate how we chose the values of the parameters used in the stretch−bend Hamiltonian (eq 4; also see eq 9).

We chose the mass parameter m for the stretch in eq 4 as the reduced mass of the C−H system, having in mind a local C−H stretch mode.

We obtained the Morse parameter D as the value of the C−H bond dissociation energy in acetylene that was determined by Habibollahzadeh et al.[47] by density functional methods. We used their value, $D = 135.5$ kcal/mol $= 47474.26$ cm^{-1}.

For the frequency of a local stretch mode, ω_s, at the bottom of the Morse potential, we use the average of the symmetric and antisymmetric stretch frequencies for acetylene. The values of $\omega_1 = 3501.537$ cm^{-1} and $\omega_3 = 3417.644$ cm^{-1} were obtained from the work of van der Pals et al.,[48] so we have $\omega_s = 3459.59$ cm^{-1}.

The Morse parameter β relates to the mass m, dissociation energy D, and harmonic frequency ω_s through the equation $\omega_s = \sqrt{2D\beta^2/m}$, from which we get the value $\beta = 1.86288 \times 10^{10}$ m^{-1}.

We define the moment of inertia in eq 4 as $I = m_H r_0^2$, by considering the bend in terms of an H atom rotating rigidly about the rest of molecule, which is treated as a fixed object. We consider r_0 to be the length of the C−H bond at equilibrium. From the ab initio calculation of Chang et al.[49] for acetylene, we get $r_0 = 1.063$ Å.

Determination of a value for the stretch−bend coupling parameter κ in eq 4 is rather complicated and occupies the rest of this Appendix. For small-amplitude motion, we have $\kappa r \sin^2 \phi \approx \kappa r \phi^2$, the form that would give a 2:1 Fermi resonance coupling. Quantum mechanically, the stretch coordinate r and bend coordinate ϕ are related to their raising and lowering operators by

$$r \approx \sqrt{\frac{\hbar}{2m\omega_s}}(a_r^\dagger + a_r)$$

$$\phi \approx \sqrt{\frac{\hbar}{2I\omega_\phi}}(a_\phi^\dagger + a_\phi) \tag{A1}$$

The coupling term can then be approximated as

$$\kappa r \sin^2 \phi \approx \kappa r \phi^2 = \kappa \sqrt{\frac{\hbar}{2m\omega_s}}\left(\frac{\hbar}{2I\omega_\phi}\right)(a_r^\dagger + a_r)(a_\phi^\dagger + a_\phi)^2 \tag{A2}$$

Now, consider the matrix element between states $|n_s, n_b\rangle = |1, 0\rangle, |0, 2\rangle$:

$$\Delta E \equiv \langle 1, 0|\, \kappa r \sin^2 \phi\, |0, 2\rangle \approx \kappa \sqrt{\frac{\hbar}{2m\omega_s}}\left(\frac{\hbar}{2I\omega_\phi}\right)\sqrt{2} \tag{A3}$$

From this relation, we get

$$\kappa \approx \sqrt{\frac{m\omega_s}{\hbar}}\left(\frac{2I\omega_\phi}{\hbar}\right)\Delta E \tag{A4}$$

We choose ω_ϕ to represent the average of the actual cis- and trans- bend frequencies for acetylene (not the frequency of the model bend potential (eq 1), which only roughly approximates the experimental bend frequency). From the work of van Ede van der Pals and Gaspard,[48] $\omega_\phi = (\omega_4 + \omega_5)/2 = 684.23$ cm^{-1}.

To get a value for κ, we must now get a reasonable value for ΔE. For guidance, we make use of the analysis of Sibert et al.[40] of the kinetic energy coupling between a stretch and a bend; we believe that this is the predominant contribution to the stretch−bend coupling in linear molecules such as acetylene. To lowest order, this coupling gives matrix elements of 2:1 form between the stretch and the bend, in a manner that is very similar to the aforementioned approximations regarding the coupling (eq 3).

Sibert et al.[40] analyzed triatomic molecules, and, of course, acetylene is a four-atom molecule. To estimate the coupling, we treat it as if it were a linear ABA molecule with A representing the H atom and B representing the C atom pair as if they were a single atom. We then follow the procedure used in ref 40 for CO_2.

The vibrational Hamiltonian for the triatomic molecule is

$$H = \frac{1}{2}\sum_{i,j}^{3} g_{ij} p_i p_j + V(x_1, x_2, x_3) \tag{A5}$$

where x_1 and x_2 are the displacement coordinates of the H atoms, and x_3 is a bend coordinate that is defined as π minus the H(CC)H angle ($x_3 = \phi$), where (CC) indicates that we treat the carbon atom pair "CC" as a single atom. The g_{ij} terms for $i, j = 1, 2, 3$ are elements of the g-matrix,[50] which is related to the inverse effective masses. The g_{ij} terms are coordinate-dependent. By expanding g_{ij} around the equilibrium coordinates $x_i = 0$ and keeping the lowest order, the kinetic energy Hamiltonian can be written as

$$T = T^0 + T^1 \tag{A6}$$

with

$$T^0 = \frac{1}{2}\mu_H p_s^2 + \frac{1}{2} g_{33}^0 p_\phi^2 \tag{A7}$$

$$T^1 = \left(\frac{\sqrt{2}\mu_{CC}}{r_0}\right)\phi p_\phi p_s - \left(\frac{\sqrt{2} g_{33}^0}{2r_0}\right) s p_\phi^2 \tag{A8}$$

where $s = (x_1 + x_2)/\sqrt{2}$ is the symmetric stretch coordinate, ϕ is the bend coordinate ($\phi = x_3$), p_s and p_ϕ are their conjugate momenta, $g_{33}^0 = g_{33}(0) = 2\mu_H/r_0^2 + 4\mu_{CC}/r_0^2$, μ_H is the inverse mass of the H atom, μ_{CC} is the inverse mass of the (CC) carbon pair, and finally r_0 is the length of the H−C bond at equilibrium.

We treat T^1 as the coupling of stretch and bend harmonic oscillators with frequencies ω_s and ω_ϕ. To calculate the contribution of T^1 analytically, we write the coordinates and momenta in eq A8 in terms of the raising and lowering operators as

$$s \approx \sqrt{\frac{\hbar\mu_H}{2\omega_s}}(a_s^\dagger + a_s)$$

$$p_s \approx i\sqrt{\frac{\hbar\omega_s}{2\mu_H}}(a_s^\dagger - a_s)$$

$$\phi \approx \sqrt{\frac{\hbar g_{33}^0}{2\omega_\phi}}(a_\phi^\dagger + a_\phi)$$

$$p_\phi \approx i\sqrt{\frac{\hbar\omega_\phi}{2g_{33}^0}}(a_\phi^\dagger - a_\phi) \quad \text{(A9)}$$

where matrix elements of the raising and lowering operators are assumed to have the standard quantum number dependence of harmonic oscillator eigenstates, but are obtained between eigenstates of the anharmonic stretch and bend, hence the approximate equalities. The terms in T^1 then become

$$\left(\frac{\sqrt{2}\mu_{CC}}{r_0}\right)\phi p_\phi p_s = -\frac{\hbar\mu_{CC}}{2r_0}\sqrt{\frac{\hbar\omega_s}{\mu_H}}(a_\phi^\dagger + a_\phi)(a_\phi^\dagger - a_\phi)(a_s^\dagger - a_s) \quad \text{(A10)}$$

$$-\left(\frac{\sqrt{2}g_{33}^0}{2r_0}\right)sp_\phi^2 = \frac{\hbar\omega_\phi}{4r_0}\sqrt{\frac{\hbar\mu_H}{\omega_s}}(a_s^\dagger + a_s)(a_\phi^\dagger - a_\phi)^2 \quad \text{(A11)}$$

For $\omega_s = 3459.59\ \text{cm}^{-1} = 6.505 \times 10^{14}$ Hz, $\omega_\phi = 684.23\ \text{cm}^{-1} = 1.2865 \times 10^{14}$ Hz, and $r_0 = 1.063 \times 10^{-10}$ m, the matrix elements between states $|1, 0\rangle$ and $|0, 2\rangle$ for the two terms are given by

$$\left\langle 1, 0\left|\left(\frac{\sqrt{2}\mu_{CC}}{r_0}\right)\phi p_\phi p_s\right|0, 2\right\rangle \simeq 9.50\ \text{cm}^{-1}$$

$$\left\langle 1, 0\left| -\left(\frac{\sqrt{2}g_{33}^0}{2r_0}\right)sp_\phi^2\right|0, 2\right\rangle \simeq 22.40\ \text{cm}^{-1}$$

Therefore,

$$\langle 1, 0|\ T^1|\ 0, 2\rangle \simeq 31.90\ \text{cm}^{-1}$$

Taking into account the double degeneracy of the bend (in the real acetylene molecule, not our two-mode model), the total contribution of the kinetic coupling is (see eq 3.6 of ref 40)

$$\sqrt{2}\,\langle 1, 0|\ T^1|\ 0, 2\rangle \approx 45.11\ \text{cm}^{-1}$$

Substituting $\Delta E = \sqrt{2}\,\langle 1, 0|T^1|0, 2\rangle \simeq 45.11\ \text{cm}^{-1}$ into eq A4, we get the value for the coupling parameter κ in the Hamiltonian eq 5:

$$\kappa \approx 2.031375 \times 10^{14}\ \text{m}^{-1}\ \text{cm}^{-1}$$

with m^{-1} denoting a true reciprocal length and cm^{-1} a unit of energy. The value of A_{sb} in the classical Hamiltonian eq 6, using β, which was previously determined in this Appendix, is then

$$A_{sb} = \frac{\kappa}{\beta} = 10904.4\ \text{cm}^{-1}$$

References and Notes

(1) Kellman, M. E. *Ann. Rev. Phys. Chem.* **1995**, *46*, 395.

(2) Kellman, M. E. Dynamical Analysis of Highly Excited Vibrational Spectra: Progress and Prospects. In *Molecular Dynamics and Spectroscopy by Stimulated Emission Pumping*; Dai, H.-L., Field, R. W., Eds.; World Scientific: Singapore, 1995.

(3) Kellman, M. E. Internal Molecular Motions. In *Encyclopedia of Chemical Physics and Physical Chemistry*; Institute of Physics: London, 2001.

(4) Kellman, M. E.; Lynch, E. D. *J. Chem. Phys.* **1986**, *85*, 5855.

(5) Xiao, L.; Kellman, M. E. *J. Chem. Phys.* **1989**, *90*, 6086.

(6) Xiao, L.; Kellman, M. E. *J. Chem. Phys.* **1990**, *93*, 5805.

(7) Svitak, J.; Li, Z.; Rose, J.; Kellman, M. E. *J. Chem. Phys.* **1995**, *102*, 4340.

(8) Lu, Z.-M.; Kellman, M. E. *J. Chem. Phys.* **1997**, *107*, 1.

(9) Keshavamurthy, S.; Ezra, G. S. *J. Chem. Phys.* **1997**, *107*, 156.

(10) Jacobson, M. P.; Jung, C.; Taylor, H. S.; Field, R. W. *J. Chem. Phys.* **1999**, *111*, 600.

(11) Joyeux, M.; Sugny, D.; Tyng, V.; Kellman, M. E.; Ishikawa, H.; Field, R. W.; Beck, C.; Schinke, R. *J. Chem. Phys.* **1999**, *112*, 4162.

(12) Keshavamurthy, S. *J. Phys. Chem. A* **2001**, *105*, 2668.

(13) Semparithi, A.; Charulatha, V.; Keshavamurthy, S. *J. Chem. Phys.* **2003**, *118*, 1146.

(14) Zhou, C.; Xie, D.; Chen, R.; Yan, G.; Guo, H.; Tyng, V.; Kellman, M. E. *Spectrochim. Acta A* **2002**, *58*, 727.

(15) Joyeux, M.; Farantos, S. C.; Schinke, R. *J. Phys. Chem. A* **2002**, *106*, 5407.

(16) Carrington, T., Jr.; Hubbard, L. M.; Schaeffer, H. F., III; Miller, W. H. *J. Chem. Phys.* **1984**, *80*, 4347.

(17) Chen, Y.; Jonas, D. M.; Kinsey, J. L.; Field, R. W. *J. Chem. Phys.* **1989**, *91*, 3976.

(18) Ervin, K. M.; Ho, J.; Lineberger, W. C. *J. Chem. Phys.* **1989**, *91*, 5974.

(19) Levin, J.; Feldman, H.; Baer, A.; Ben-Hamu, D.; Heber, O.; Zajfman, D.; Vager, Z. *Phys. Rev. Lett.* **1998**, *81*, 3347.

(20) Stanton, J. F.; Gauss, J. *J. Chem. Phys.* **1999**, *110*, 1831.

(21) Hayes, R. L.; Fattal, E.; Govind, N.; Carter, E. A. *J. Am. Chem. Soc.* **2001**, *123*, 641.

(22) Zou, S.; Bowman, J. M. *J. Chem. Phys.* **2002**, *116*, 6667.

(23) Bowman, J. M.; Gazdy, B.; Bentley, J. A.; Lee, T. J.; Dateo, C. E. *J. Chem. Phys.* **1993**, *99*, 308.

(24) Bowman, J. M.; Irle, S.; Morokuma, K.; Wodtke, A. *J. Chem. Phys.* **2001**, *114*, 7923.

(25) Xu, D.; Xie, D.; Guo, H. *J. Phys. Chem. A* **2002**, *106*, 10174.

(26) Davis, M. J.; Heller, E. J. *J. Chem. Phys.* **1981**, *75*, 246.

(27) Sibert, E. L., III; Reinhardt, W. P.; Hynes, J. T. *J. Chem. Phys.* **1982**, *77*, 3583.

(28) Kellman, M. E. *J. Chem. Phys.* **1985**, *83*, 3843.

(29) Heller, E. J. *J. Phys. Chem.* **1995**, *99*, 2625.

(30) Rose, J. P.; Kellman, M. E. *J. Chem. Phys.* **1996**, *105*, 7348.

(31) Wu, G. *Chem. Phys. Lett.* **1998**, *292*, 369.

(32) Rose, J. P.; Kellman, M. E. *J. Phys. Chem. A* **2000**, *104*, 10471.

(33) Kellman, M. E.; Rose, J. P.; Tyng, V. *Eur. Phys. J. D* **2001**, *14*, 225.

(34) Jacobson, M. P.; Child, M. S. *J. Chem. Phys.* **2001**, *114*, 250.

(35) Jacobson, M. P.; Child, M. S. *J. Chem. Phys.* **2001**, *114*, 262.

(36) Billing, G. D.; Mikkelsen, K. V. Chapter 7. In *Advanced Molecular Dynamics and Chemical Kinetics*; Wiley: New York, 1997.

(37) Halonen, L.; Child, M. S.; Carter, S. *Mol. Phys.* **1982**, *47*, 1097.

(38) Murrell, J. N.; Carter, S.; Farantos, S. C.; Huxley, P.; Varandas, A. J. C. *Molecular Potential Energy Functions*; Wiley−Interscience: New York, 1984.

(39) Bentley, J. A.; Wyatt, R. E.; Menou, M.; Leforestier, C. *J. Chem. Phys.* **1992**, *97*, 4255.

(40) Sibert, E. L.; Hynes, J. T.; Reinhardt, W. P. *J. Phys. Chem.* **1983**, *87*, 2032.

(41) Dahl, J. P.; Springborg, M. *J. Chem. Phys.* **1988**, *88*, 4535.

(42) Vasan, V. S.; Cross, R. J. *J. Chem. Phys.* **1983**, *78*, 3869.

(43) Gallas, J. A. C. *Phys. Rev. A* **1980**, *21*, 1829.

(44) Sage, M. L. *Chem. Phys.* **1978**, *35*, 375.

(45) Dixon, R. N. *Trans. Faraday Soc.* **1964**, *60*, 1363.

(46) Laidler, K. J. *Chemical Kinetics*; 3rd ed.; Harper and Row: New York, 1987.

(47) Habibollahzadeh, D.; Murray, J. S.; Grodzicki, M.; Seminario, J. M.; Politzer, P. *Int. J. Quantum Chem.* **1992**, *42*, 267.

(48) van Ede van der Pals, P.; Gaspard, P. *J. Chem. Phys.* **1999**, *110*, 5619.

(49) Chang, N.-Y.; Shen, M.-Y.; Yu, C.-H. *J. Chem. Phys.* **1997**, *106*, 3237.

(50) Wilson, E. B., Jr.; Decius, J. C.; Cross, P. C. *Molecular Vibrations*; McGraw−Hill: New York, 1955.